Construction of Solutions to Electromagnetic Problems in Terms of Two Collinear Vector Potentials

Natalia K. Georgieva, *Member, IEEE*

***Abstract*—In this paper, the construction of solutions to transient electromagnetic (EM) problems in terms of two collinear vector potentials (VPs) is subjected to a careful theoretical study and numerical verification. The analysis concerns a general isotropic medium that can be inhomogeneous, lossy, and may contain sources. It is also assumed that the medium has instantaneous response, i.e., its EM properties are frequency independent. First, the completeness of the solution in terms of the two VPs in homogeneous and inhomogeneous media is addressed. Second, the behavior of the VPs at interfaces and edges is considered. Finally, a number of simple, but relevant numerical tests are performed to verify the theoretical model. This paper is part of the effort to establish the theoretical background of a novel efficient approach to the analysis of transient EM propagation based on the VPs.**

***Index Terms*—Electromagnetic potentials, electromagnetic transient analysis, FDTD methods.**

I. Introduction

IT IS well known that the electromagnetic (EM) field can be described not only in terms of the field vectors, but also in terms of vector and scalar potentials. In [1], the following has been stated for time–harmonic fields in an isotropic medium, but it is also true in the general transient case: "an arbitrary field in a homogeneous source-free region can be expressed as a sum of a TM field and a TE field." The TM (with respect to the distinguished direction of an arbitrary unit vector $\hat{c}$) field is described by the magnetic vector potential (VP) $\vec{A} = \hat{c}A$, while the TE field is described by the electric VP $\vec{F} = \hat{c}F$. Both potentials are solutions of the wave equation in the time domain (or the Helmholtz' equation in the frequency domain). Both vectors are collinear of fixed direction $\hat{c}$. The scalars A and F will be referred to as wave potentials (WPs).

A similar concept is addressed in [2], where a robust mathematical proof can be found for the representation of the EM field in terms of two scalar quantities, which are the magnitudes of two collinear Hertz potentials (the electric Hertz potential Π_e and the magnetic Hertz potential Π_m) in an isotropic homogeneous source-free medium. In fact, the concept can be traced back to 1904, when Whittaker proved that "only two functions are actually necessary (in place of four)," i.e., $(\vec{A}, \Phi)$, to describe the EM field associated with any configuration of moving or static charges (see [3]).

It should be recognized that the concept of TE/TM decomposition (or scalarization) of the EM field has often been revisited by researchers in the field of theoretical electromagnetism and complex media electromagnetism. This subject is rather broad and the interested reader is referred to just very few relevant papers [4]–[7], which provide both comprehensive coverage of the new developments in the field and extensive lists of references. At the same time, the approaches of modern computational electromagnetics are almost exclusively based on models, which treat the field vectors directly: the system of Maxwell's equations or its equivalent integral equations. This paper will consider the concept of EM scalarization from the point-of-view of computational electrodynamics. However, its purpose is not the introduction of yet another time-domain analysis approach. It is the hope of the author that this paper will help to add more light onto the subject of EM potentials, their significance, and usefulness, especially from a computational point-of-view.

To the author's knowledge, the formulation of a numerical approach to the solution of a general (lossy, inhomogeneous, involving sources) transient EM problem in terms of VPs has never been considered in detail. A possible reason is that it was deemed too complicated for practical purposes. Moreover, the solution to a transient EM problem in terms of two scalar potentials (the WPs) has always been dismissed as an impossible task. However, as it will be shown below, the general analysis reveals interesting properties of the VP model, which make its implementation in practical numerical algorithms feasible and very promising in a wide class of problems.

Recently, solid mathematical work was done on the scalarization of time–harmonic EM fields [8] in inhomogeneous uniaxial problems involving sources, which clearly proves that the TE/TM decomposition with respect to a distinguished axis is possible in inhomogeneous media as long as the distinguished axis is parallel to the gradient of the material inhomogeneity. The fundamental concepts of the work presented here were developed independently from the one reported in [8]. That is why it carries a number of different original features. First, it was developed directly in the time domain, making the assumption for an instantaneous response (the material characteristics of the medium are assumed frequency independent). This limitation is common in most conventional time-domain algorithms used in high-frequency computer-aided design (CAD). Second, the current approach is based on a more general analysis, which initially considers all six components of the two VPs $\vec{A}$ and

Manuscript received June 30, 2001. This work was supported in part by the Natural Sciences and Engineering Research Council of Canada under Grant 227660-00, and in part by Micronet under Grant C.6.NN/NCE00.

The author is with the Department of Electrical and Computer Engineering, McMaster University, Hamilton, ON, Canada L8S 4K1 (e-mail: talia@mcmaster.ca).

Publisher Item Identifier 10.1109/TMTT.2002.801343.

$\vec{F}$. It shows explicitly the conditions under which the TE/TM decomposition is possible. It also shows the conditions under which scalarization is not possible, as well as the way the coupling of all modes occurs under these conditions. In contrast, in [8], the scalarization is carried out by the introduction of auxiliary potentials Ψ and Θ via the two-dimensional version of the Helmholtz theorem, which is applied to the $\hat{c}$ transverse-field components. Nevertheless, it can be shown that the pair $\hat{c}(\Psi, \Theta)$ is equivalent to the pair $\hat{c}(A_\mu, F_\varepsilon)$ introduced later in this paper. Third, the proposed technique uses VP pairs of changing direction, which can handle the solution of lossy inhomogeneous problems with more than one direction of the gradient of the material constants. The equations describing the transition between orthogonal VP pairs are developed and the issues related to the uniqueness of the solution are addressed. Lastly, this theoretical model has been implemented in a finite-difference algorithm, which, in the time domain, can solve a wide class of problems involving homogeneous and partly inhomogeneous (e.g., layered) media with metallic inclusions of any shape, and which has considerably improved efficiency in comparison with the conventional finite-difference time-domain (FDTD) algorithm.

This paper has its roots in previous research, which resulted in the development of a time-domain algorithm based on the magnetic VP $\vec{A}$ and the second-order wave equation [9]. It was the first successful attempt to implement the VP concept into a FDTD algorithm. DeFlaviis *et al.* [10] and Diaz *et al.* [11] also reported a transient analysis algorithm based on an auxiliary VP $\vec{K}$, which is governed by the vector wave equation.

It must be noted, however, that these VP approaches were not the first to apply FDTD algorithms to the solution of the second-order wave equation. Krupežević *et al.* [12] proposed the wave-equation FDTD method to the analysis of waveguide structures based on the vector wave equation for the $\vec{E}$ vector, which leads to three coupled scalar wave equations. Aoyagi *et al.* [13] also used the second-order wave equation in a hybrid algorithm. It solved Maxwell's equations or the vector-wave equation (for $\vec{E}$ or $\vec{H}$) in inhomogeneous regions of the problem space, but used two scalar wave equations in homogeneous ("divergence-free") regions. The two scalar wave equations described the propagation of two field components only (either magnetic or electric), which had to be tangential to the subregion's boundary. From this early work, it became clear that the vector wave equation for one of the field vectors does not offer any advantages in comparison with the Yee-cell FDTD method in the general three-dimensional inhomogeneous case. However, it can offer up to 30% reduction in CPU time if predominantly homogeneous problems are analyzed where planar partitioning between regions is possible (i.e., layered structures). The savings are due to the fact that, in homogeneous regions with infinite planar boundaries of the same unit normal $\hat{n}$, the field behavior is entirely represented by only two scalar quantities (either $\hat{n} \times \vec{H}$ or $\hat{n} \times \vec{E}$) and their scalar wave equations.

The first applications of a pair of collinear VPs of fixed direction, which solved the wave equations for only two scalar WPs, were shown just recently [14]. The first finite-difference implementation showed that general inhomogeneous problems could be solved in terms of two scalar quantities. The theoretical estimate of the CPU time and memory requirements of the time-domain wave-potential (TDWP) algorithm in comparison with Yee's FDTD algorithm [15] gives a reduction of at least one-third in the *general case*, which is due to the reduced number of unknowns.

These first applications [14], however, revealed several problems, which needed further careful study. The choice of the direction of the VPs was crucial when dielectric interfaces were present, especially between regions, whose dielectric constants would differ significantly. This choice was also important when corners and edges were present. It became obvious that the bottleneck is the formulation of the boundary conditions (BCs) for the VPs. Thus, it became imperative to develop a general model of the VP propagation, which could give a clear picture of their behavior at material interfaces and inhomogeneities.

II. General VP Equations

One starts with the classical introduction of the magnetic VP $\vec{A}$ and the electric VP $\vec{F}$ as

$$\vec{H}^A = \frac{1}{\mu} \nabla \times \vec{A} \quad \vec{E}^F = -\frac{1}{\varepsilon} \nabla \times \vec{F}. \tag{1}$$

Here, $\vec{H}^A$ is the magnetic-field vector of a field associated with electric sources only ($\nabla \cdot \vec{B}^A = 0$). The $\vec{E}^F$ vector is the electric field associated with magnetic sources only ($\nabla \cdot \vec{D}^F = 0$). Their counterparts $\vec{E}^A$ and $\vec{H}^F$ will be found by substitution in Maxwell's equations. The total field is a superposition of $(\vec{E}^A, \vec{H}^A)$ and $(\vec{E}^F, \vec{H}^F)$. Note that this implies linear media. The next step is to substitute (1) in Maxwell's equations and split them into two systems of equations as follows:

$$\begin{aligned} \nabla \times \vec{H}^F &= -\nabla \times \partial_t \vec{F} - \nabla \times \left(\frac{\sigma}{\varepsilon} \vec{F}\right) + \nabla \\ &\quad \times \left[\left(\nabla \frac{1}{\mu}\right) \times \vec{A}\right] \\ \mu \partial_t \vec{H}^F &= \nabla \times \nabla \times \frac{\vec{F}}{\varepsilon} - \sigma_m \vec{H}^F + \left(\nabla \frac{\sigma_m}{\mu}\right) \times \vec{A} - \vec{J}_m^i \end{aligned} \tag{2}$$

$$\begin{aligned} \varepsilon \partial_t \vec{E}^A &= \nabla \times \nabla \times \frac{\vec{A}}{\mu} - \sigma \vec{E}^A - \left(\nabla \frac{\sigma}{\varepsilon}\right) \times \vec{F} - \vec{J}^i \\ \nabla \times \vec{E}^A &= -\nabla \times \partial_t \vec{A} - \nabla \times \left[\left(\nabla \frac{1}{\varepsilon}\right) \times \vec{F}\right] \\ &\quad -\nabla \times \left(\frac{\sigma_m}{\mu} \vec{A}\right). \end{aligned} \tag{3}$$

From the first equation in (2), it follows that

$$\vec{H}^F = -\partial_t \vec{F} - \frac{\sigma}{\varepsilon} \vec{F} - \nabla \Psi + \left(\nabla \frac{1}{\mu}\right) \times \vec{A} \tag{4}$$

and from the second equation in (3), it follows that

$$\vec{E}^A = -\partial_t \vec{A} - \frac{\sigma_m}{\mu} \vec{A} - \nabla \Phi - \left(\nabla \frac{1}{\varepsilon}\right) \times \vec{F}. \tag{5}$$

Here, Ψ and Φ are the magnetic scalar potential and electric scalar potential, respectively. Note the cross-coupling between the F-field and the A-potential and the A-field and the F-potential due to the constants' nonzero gradients in (4) and (5).

To complete this analysis, the components of the total field $(\vec{E}, \vec{H})$ will be expressed in terms of the VPs $\vec{A}$ and $\vec{F}$. Making use of (1), (4), and (5), one arrives at the following field-to-potential relations:

$$\vec{E} = \vec{E}^A + \vec{E}^F = -\mathfrak{T}_\mu\left\{\vec{A}_\mu\right\} - \nabla\Phi - \nabla\times\vec{F}_\varepsilon$$
$$\vec{H} = \vec{H}^A + \vec{H}^F = -\mathfrak{T}_\varepsilon\left\{\vec{F}_\varepsilon\right\} - \nabla\Psi + \nabla\times\vec{A}_\mu. \quad (6)$$

Here, the potential functions

$$\vec{A}_\mu = \vec{A}/\mu \quad (A)$$
$$\vec{F}_\varepsilon = \vec{F}/\varepsilon \quad (V) \quad (7)$$

have been introduced. $\mathfrak{T}_\varepsilon$ and $\mathfrak{T}_\mu$ are first-order linear differential operators in time

$$\mathfrak{T}_\varepsilon = \varepsilon\partial_t + \sigma$$
$$\mathfrak{T}_\mu = \mu\partial_t + \sigma_m \quad (8)$$

which make the equations compact and convenient to manipulate.

Alternatively, one may use (1), the second equation of (2), and the first equation of (3) to derive the equivalent to (6) relations

$$\mathfrak{T}_\varepsilon\left\{\vec{E}\right\} = \nabla\times\left(\nabla\times\vec{A}_\mu - \mathfrak{T}_\varepsilon\left\{\vec{F}_\varepsilon\right\}\right) - \vec{J}^i$$
$$\mathfrak{T}_\mu\left\{\vec{H}\right\} = \nabla\times\left(\nabla\times\vec{F}_\varepsilon + \mathfrak{T}_\mu\left\{\vec{A}_\mu\right\}\right) - \vec{J}^i_m. \quad (9)$$

The wave equations governing the potentials are readily derived from (6) and (9) as follows:

$$\nabla\times\nabla\times\vec{A}_\mu + \mathfrak{T}^2_{\mu\varepsilon}\left\{\vec{A}_\mu\right\} + \mathfrak{T}_\varepsilon\{\nabla\Phi\} - (\nabla\mathfrak{T}_\varepsilon)\times\left\{\vec{F}_\varepsilon\right\} = \vec{J}^i$$
$$\nabla\times\nabla\times\vec{F}_\varepsilon + \mathfrak{T}^2_{\mu\varepsilon}\left\{\vec{F}_\varepsilon\right\} + \mathfrak{T}_\mu\{\nabla\Psi\} + (\nabla\mathfrak{T}_\mu)\times\left\{\vec{A}_\mu\right\} = \vec{J}^i_m. \quad (10)$$

Here, $\mathfrak{T}^2_{\mu\varepsilon}$ is the second-order differential operator in time

$$\mathfrak{T}^2_{\mu\varepsilon} = \mathfrak{T}_\mu\mathfrak{T}_\varepsilon = \mu\varepsilon\partial^2_{tt} + (\varepsilon\sigma_m + \mu\sigma)\partial_t + \sigma\sigma_m. \quad (11)$$

The vector operators $(\nabla\mathfrak{T}_\varepsilon)$ and $(\nabla\mathfrak{T}_\mu)$ are the gradients of the operators defined in (8) so that, e.g.,

$$(\nabla\mathfrak{T}_\varepsilon)\times\left\{\vec{F}_\varepsilon\right\} = (\nabla\varepsilon)\times\partial_t\vec{F}_\varepsilon + (\nabla\sigma)\times\vec{F}_\varepsilon. \quad (12)$$

If one applies the generalized Lorenz gauge to the potentials $\vec{A}_\mu$ and $\vec{F}_\varepsilon$

$$\nabla\cdot\vec{A}_\mu = -\mathfrak{T}_\varepsilon\{\Phi\} \quad \nabla\cdot\vec{F}_\varepsilon = -\mathfrak{T}_\mu\{\Psi\} \quad (13)$$

their general wave equations are obtained as

$$\nabla^2\vec{A}_\mu - \mathfrak{T}^2_{\mu\varepsilon}\left\{\vec{A}_\mu\right\} + (\nabla\mathfrak{T}_\varepsilon)\{\Phi\} + (\nabla\mathfrak{T}_\varepsilon)\times\left\{\vec{F}_\varepsilon\right\} = -\vec{J}^i$$
$$\nabla^2\vec{F}_\varepsilon - \mathfrak{T}^2_{\mu\varepsilon}\left\{\vec{F}_\varepsilon\right\} + (\nabla\mathfrak{T}_\mu)\{\Psi\} - (\nabla\mathfrak{T}_\mu)\times\left\{\vec{A}_\mu\right\} = -\vec{J}^i_m. \quad (14)$$

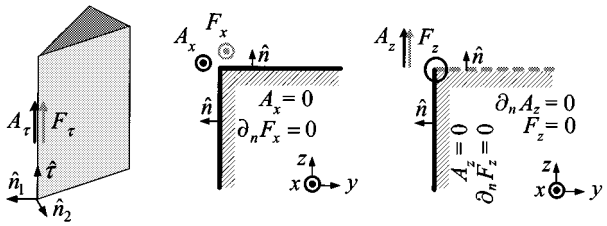

(a) (b) (c)

Fig. 1. BCs of the VP components at perfectly conducting edges.

Notice the cross-coupling between the magnetic and electric potentials in the case of nonzero gradients of the constitutive parameters of the medium. In the case of a homogeneous medium, (14) defaults to the well-known wave equations.

The following important conclusions can be made from (14). First, collinear VPs, which are normal to material interfaces, are not mutually coupled. The scattering of the EM field at an orthogonal to the VP pair interface can be fully described by two scalar quantities, i.e., the magnitudes of the VPs. However, if the VP pair has tangential components at an interface, they will be mutually coupled. They will also be indirectly coupled to their normal components. One has to consider all six coupled components, which makes the problem too complicated. Second, a component of a VP, which is normal to an interface, will never give rise to a tangential component of its own. On the contrary, a component of a VP, which is tangential to a dielectric interface $\vec{A}_\tau$, will generate a normal component A_n. The same holds for $\vec{F}$ at magnetic interfaces.

Further analysis shows that the BCs at conducting edges of a pair of VPs, which are tangential to the edge [see Fig. 1(a)], are well posed. A homogeneous Dirichlet condition is imposed on the tangential magnetic VP $A_\tau = 0$, regardless of the direction from which the edge is approached. A homogeneous Neumann condition is imposed on the tangential electric VP $\partial F_\tau/\partial n = 0$, where $\hat{n}$ is *any* direction normal to the edge [see Fig. 1(b)]. On the contrary, if a VP is orthogonal to the edge, its BCs are ill posed. They do depend on the direction from which the edge is approached. For example, at an x-directed right-angle wedge, $\partial F_z/\partial y = 0$, when the observation point approaches the edge along the z-axis [see Fig. 1(c)]. However, when the observation point approaches the edge along the y-axis, the BC is a Dirichlet one, i.e., $F_z = 0$. Such ill-posed BCs degrade the performance of numerical algorithms based on finite discrete meshes.

To summarize, if one can keep the VPs normal to interfaces and tangential to edges and wedges, two scalar quantities (the magnitudes of two collinear VPs) will be sufficient to describe the total field behavior without having to take care of mode coupling. It is now obvious that, in order to solve practical problems involving material interfaces, edges, and corners in a robust and simple manner, one cannot keep the direction of the VP pair constant in space.

III. Mode Equivalence

The above conclusion makes it imperative to study the transitions between pairs of collinear VPs. These transitions are possible and there are clear rules to carry them out, at least in the case of mutually orthogonal VP pairs. Thus, the computational

TABLE I
SUMMARY OF THE MODE EQUIVALENCE FORMULAS IN HOMOGENEOUS REGIONS

(A_x, F_x)	(A_y, F_y)	(A_z, F_z)
$\left.\begin{matrix}(-\partial_{xx}^2+\mathfrak{T}_{\mu\varepsilon}^2)\{A_{\mu x}\}\\ \nabla_{yz}^2\{A_{\mu x}\}\end{matrix}\right\}$	$-\partial_{xy}^2 A_{\mu y}-\partial_z\left(\mathfrak{T}_\varepsilon\{F_{\varepsilon y}\}\right)$	$-\partial_{xz}^2 A_{\mu z}+\partial_y\left(\mathfrak{T}_\varepsilon\{F_{\varepsilon z}\}\right)$
$-\partial_{yx}^2 A_{\mu x}+\partial_z\left(\mathfrak{T}_\varepsilon\{F_{\varepsilon x}\}\right)$	$\left.\begin{matrix}(-\partial_{yy}^2+\mathfrak{T}_{\mu\varepsilon}^2)A\\ \nabla_{xz}^2\{A_{\mu y}\}\end{matrix}\right\}$	$-\partial_{yz}^2 A_{\mu z}-\partial_x\left(\mathfrak{T}_\varepsilon\{F_{\varepsilon z}\}\right)$
$-\partial_{zx}^2 A_{\mu x}-\partial_y\left(\mathfrak{T}_\varepsilon\{F_{\varepsilon x}\}\right)$	$-\partial_{zy}^2 A_{\mu y}+\partial_x\left(\mathfrak{T}_\varepsilon\{F_{\varepsilon y}\}\right)$	$\left.\begin{matrix}(-\partial_{zz}^2+\mathfrak{T}_{\mu\varepsilon}^2)A_{\mu z}\\ \nabla_{xy}^2\{A_{\mu z}\}\end{matrix}\right\}$
$\left.\begin{matrix}(-\partial_{xx}^2+\mathfrak{T}_{\mu\varepsilon}^2)F_{\varepsilon x}\\ \nabla_{yz}^2\{F_{\varepsilon x}\}\end{matrix}\right\}$	$\partial_z\left(\mathfrak{T}_\mu\{A_{\mu y}\}\right)-\partial_{xy}^2 F_{\varepsilon y}$	$-\partial_{xz}^2 F_{\varepsilon z}-\partial_y\left(\mathfrak{T}_\mu\{A_{\mu z}\}\right)$
$-\partial_{yx}^2 F_{\varepsilon x}-\partial_z\left(\mathfrak{T}_\mu\{A_{\mu x}\}\right)$	$\left.\begin{matrix}(-\partial_{yy}^2+\mathfrak{T}_{\mu\varepsilon}^2)F_{\varepsilon y}\\ \nabla_{xz}^2\{F_{\varepsilon y}\}\end{matrix}\right\}$	$-\partial_{yz}^2 F_{\varepsilon z}+\partial_x\left(\mathfrak{T}_\mu\{A_{\mu z}\}\right)$
$-\partial_{zx}^2 F_{\varepsilon x}+\partial_y\left(\mathfrak{T}_\mu\{A_{\mu x}\}\right)$	$-\partial_x\left(\mathfrak{T}_\mu\{A_{\mu y}\}\right)-\partial_{zy}^2 F_y$	$\left.\begin{matrix}(-\partial_{zz}^2+\mathfrak{T}_{\mu\varepsilon}^2)F_{\varepsilon z}\\ \nabla_{xy}^2\{F_{\varepsilon z}\}\end{matrix}\right\}$

Note: $\nabla_{\xi\eta}^2=\partial_{\xi\xi}^2+\partial_{\eta\eta}^2$

region can be divided into domains of constant direction of the VP pair, such that mode coupling is avoided. This mode coupling will be taken care of in an implicit manner by the transition equations at the mutual boundaries of the neighboring domains.

One needs to establish the equations, which will allow the seamless transition between orthogonal VP pairs, so that the direction of the VP pair can be changed according to the gradient of the EM constants in a given domain. Assume that a pair $(A_{\mu x}, F_{\varepsilon x})$ is to be rotated to a $(A_{\mu y}, F_{\varepsilon y})$ pair or to a $(A_{\mu z}, F_{\varepsilon z})$ pair in a neighboring domain. This has to be done in such a way that the field components expressed in terms of the $(A_{\mu x}, F_{\varepsilon x})$ pair are the same as those expressed in terms of the orthogonal pair [either $(A_{\mu y}, F_{\varepsilon y})$ or $(A_{\mu z}, F_{\varepsilon z})$] at the domain's boundary. The field components are expressed in terms of their respective potentials using (6) and (9). The transition from one pair to another is done using the modes' longitudinal field components, which depend on a single potential. Thus, the WPs of a VP pair at the boundary of a domain are calculated independently from each other, which is convenient for practical implementations.

For example, in homogeneous and source-free regions, the transition equations are based on the field-to-potential relations summarized in Table I. The expressions in Table I can be easily expanded to include the case of inhomogeneous lossy regions, as they follow from the general formulas in (6) and (9). It will be reiterated that only the two longitudinal field components (H_ξ and E_ξ, $\xi \equiv x$, or y, or z) are used to calculate the VP pair $(A_{\mu\xi}, F_{\varepsilon\xi})$ at the domain's boundary (see the highlighted formulas in Table I). Once the WPs are computed at the domain's boundary, their respective wave equations are solved within its volume.

To illustrate the concept, let us consider the computation of the $(A_{\mu x}, F_{\varepsilon x})$ pair at a flat domain boundary. If the boundary's normal is $\hat{n} \equiv \pm\hat{x}$, then the two-dimensional Poisson equations

$$\nabla_{yz}^2 A_{\mu x} = g^A \quad \nabla_{yz}^2 F_{\varepsilon x} = g^F \tag{15}$$

must be solved, where g^A and g^F represent source functions depending on the orthogonal VP pair of the neighboring domain. For example, if the neighboring VP pair is $(A_{\mu y}, F_{\varepsilon y})$, then

$$g^A = -\partial_{xy}^2 A_{\mu y} - \partial_z\Big(\mathfrak{T}_\varepsilon\{F_{\varepsilon y}\}\Big)$$
$$g^F = -\partial_{xy}^2 F_{\varepsilon y} + \partial_z\Big(\mathfrak{T}_\mu\{A_{\mu y}\}\Big). \tag{16}$$

If the boundary normal is orthogonal to the direction of the VP pair $\hat{n}\perp\hat{x}$, then the $(A_{\mu x}, F_{\varepsilon x})$ pair is computed from the equations

$$-\partial_{xx}^2 A_{\mu x} + \mathfrak{T}_{\mu\varepsilon}^2\{A_{\mu x}\} = g^A$$
$$-\partial_{xx}^2 F_{\varepsilon x} + \mathfrak{T}_{\mu\varepsilon}^2\{F_{\varepsilon x}\} = g^F. \tag{17}$$

There are three important notes to be made here with respect to the finite-difference implementation of the transition equations (15)–(17). First, the matrices arising from the discretization of the two-dimensional Poisson equations in (15) are inverted offline, as a pre-process to the time-stepping analysis. They depend solely on the size and shape of the domain's boundary. Second, the equations in (17) are solved with an explicit standard second-order-accuracy scheme [16]. Third, any combination of (15) and (17) can be used at any portion of the domain's boundary, which is convenient for the particular geometry and the BCs of the problem.

In effect, the VP pair transition equations discussed above set up the BCs for two collinear field components (H_ξ, E_ξ). The question is whether such BCs ensure the uniqueness of the solution in the given domain. The answer to this question is positive and the proof is based on the uniqueness theorem.

IV. UNIQUENESS OF THE SOLUTION IN TERMS OF WPs

The uniqueness theorem in electromagnetics gives the conditions under which the system of Maxwell's equations will generate only one possible solution to a given problem. Its mathematical formulation is given in many sources (see, e.g., [1] or [17]), and it follows from the integral equation:

$$\oiint_S \left(\delta\vec{E}\times\delta\vec{H}^*\right)\cdot d\vec{s} + \iiint_{V_{[S]}} \left[(\sigma+j\omega\tilde{\varepsilon})^*\left|\delta\vec{E}\right|^2 + j\omega\tilde{\mu}\left|\delta\vec{H}\right|^2\right] dv = 0 \tag{18}$$

where

σ specific conductivity;
$\tilde{\varepsilon}$ $= \varepsilon' - j\varepsilon''$ is complex dielectric permittivity;
$\tilde{\mu}$ $= \mu' - j\mu''$ is complex magnetic permeability.

The vectors $\delta\vec{E}$ and $\delta\vec{H}$ represent the difference field of two solutions, which are presumed to exist for the same problem (same equations, same BCs, and same sources). If one can en-

sure that

$$\oiint_S \left(\delta\vec{E}\times\delta\vec{H}^*\right)\cdot d\vec{s}=0 \tag{19}$$

then the volume integral in (18) will vanish, which is possible only if both $|\delta\vec{E}|$ and $|\delta\vec{H}|$ are zero throughout the volume $V_{[S]}$. Thus, (19) guarantees the uniqueness of the solution.

The classical interpretation of (19) relies on the vector identities

$$\hat{n}\cdot\left(\delta\vec{E}\times\delta\vec{H}^*\right)=\delta\vec{E}\cdot\left(\delta\vec{H}^*\times\hat{n}\right)=\delta\vec{H}^*\cdot\left(\hat{n}\times\delta\vec{E}\right). \tag{20}$$

They lead to the conclusion that a unique solution to an EM problem exists if *one* of the following BCs is specified over any part of the boundary *S*: the tangential vector $\vec{E}_\tau$ (which sets $\delta\vec{E}_\tau=0$) or the tangential vector $\vec{H}_\tau$ (which sets $\delta\vec{H}_\tau=0$).

Below it will be shown that there are other cases satisfying (19), which should be added to the list of valid BCs. Moreover, we will give a new interpretation of all cases in terms of TE/TM modes with respect to a distinguished direction (the direction of the VP pair).

Let us first represent the difference field ($\delta\vec{E}$, $\delta\vec{H}$) with its three components with respect to the local coordinate system ($\hat{n}$, $\hat{\tau}_1$,$\hat{\tau}_2$) at a point on the surface, where $\hat{n}=\hat{\tau}_1\times\hat{\tau}_2$ is the unit normal vector. One can then expand the integrand of (19) as

$$\left(\delta\vec{E}\times\delta\vec{H}^*\right)\cdot\hat{n}=\delta E_{\tau_1}\delta H^*_{\tau_2}-\delta E_{\tau_2}\delta H^*_{\tau_1}. \tag{21}$$

From (21), it is obvious that specifying *one* of the following BCs over any part of the boundary surface *S* can also ensure the uniqueness of the solution: the collinear tangential-field components (E_{τ_1}, H_{τ_1}), which sets $\delta E_{\tau_1}=0$ and $\delta H_{\tau_1}=0$, or the collinear tangential-field components (E_{τ_2}, H_{τ_2}), which sets $\delta E_{\tau_2}=0$ and $\delta H_{\tau_2}=0$.

Let us now assume that the BCs for the two normal to the surface field components (D_n, B_n) are specified over a part of the boundary, which we will denote as S_n. Below, we will show that this is a valid BC according to the uniqueness theorem as long as the constitutive parameters remain constant over S_n. The above assumption means that the difference field has no normal components at the boundary surface S_n

$$\delta D_n=0 \text{ and } \delta B_n=0 \text{ over } S_n. \tag{22}$$

From Maxwell's equations, it follows that the remaining tangential components of the difference field satisfy the two-dimensional Laplace equation over S_n. Notice that (22) is equivalent to defining the difference field as a TEM_n wave, which is known to have tangential-field components satisfying the two-dimensional Laplace equation in the $\hat{n}$-transverse plane. Nevertheless, we will show that the above statement is true. For example, let us consider the $\delta\vec{H}_\tau$ vector. The difference field does not have sources, therefore, $\nabla\cdot\delta\vec{B}_\tau=0$. Assume that $\nabla_\perp\mu=0$ over S_n, where $\nabla_\perp$ denotes the gradient operator with respect to the tangential to the surface coordinates (τ_1, τ_2). The following is then true over S_n:

$$\nabla_\perp\cdot\delta\vec{H}_\tau=0. \tag{23}$$

Taking the two-dimensional gradient $\nabla_\perp$ of (23) leads to the equation

$$\nabla_\perp\times\nabla_\perp\times\delta\vec{H}_\tau+\nabla^2_\perp\delta\vec{H}_\tau=0. \tag{24}$$

The $\nabla_\perp\times\delta\vec{H}_\tau$ vector has only a normal component, which is identical to the normal component of the full curl of the $\delta\vec{H}_\tau$ field $(\nabla\times\delta\vec{H}_\tau)_n$. Thus,

$$(\nabla_\perp\times\delta\vec{H}_\tau)_n\equiv(\nabla\times\delta\vec{H}_\tau)_n=j\omega(\delta D_n). \tag{25}$$

However, it has been assumed that $\delta D_n=0$ everywhere on S_n. It follows that the $\delta\vec{H}_\tau$ field satisfies the two-dimensional Laplace equation over the boundary portion S_n

$$\nabla^2_\perp\delta\vec{H}_\tau=0 \text{ over } S_n. \tag{26}$$

In a dual manner, one can show that if (22) holds over the boundary portion S_n, the $\delta\vec{E}_\tau$ field also satisfies the two-dimensional Laplace equation

$$\nabla^2_\perp\delta\vec{E}_\tau=0 \text{ over } S_n. \tag{27}$$

Equations (26) and (27) will ensure vanishing tangential components of the difference field over S_n only if the BCs complementing (26) and (27) are homogeneous Dirichlet ones along the contour C_n bounding S_n, i.e., $\delta\vec{E}_\tau=0$ or $\delta\vec{H}_\tau=0$ along C_n. This condition is satisfied if S_n is surrounded by portions of the boundary surface where the tangential field components' boundary values are set. Thus, specifying the two collinear normal field components (D_n, B_n) over a part of the boundary surface is a valid BC, which ensures the uniqueness of the solution provided that the tangential gradients of the material constants over S_n are zero. Specifying (D_n, B_n) over the whole *closed* boundary surface does not guarantee vanishing $\delta\vec{E}_\tau$ and $\delta\vec{H}_\tau$. Moreover, according to the uniqueness theorem of Laplace equation, (26) and (27) will not have unique solutions themselves. In order for a unique solution to (26) and (27) to exist, at least one point on the boundary surface S_n (or its contour C_n if S_n is open) must have the function's value specified. In order for this unique solution to be a trivial one, this function boundary value must be zero, and the BCs at all other contour points (if S_n is open) must be homogeneous.

To summarize, one must specify one of the following: (E_{τ_1}, E_{τ_2}), or (H_{τ_1}, H_{τ_2}) or (E_{τ_1}, H_{τ_1}) or (E_{τ_2}, H_{τ_2}) for at least one point on the boundary surface S. On the remainder of it, one can set either the values of the normal pair (D_n, B_n) or the values of any of the above pairs.

The BCs in terms of two collinear field vectors (E_ξ, H_ξ) over the domain surface S in effect set the boundary values for the respective VP pair (A_ξ, F_ξ). Thus, the two potential

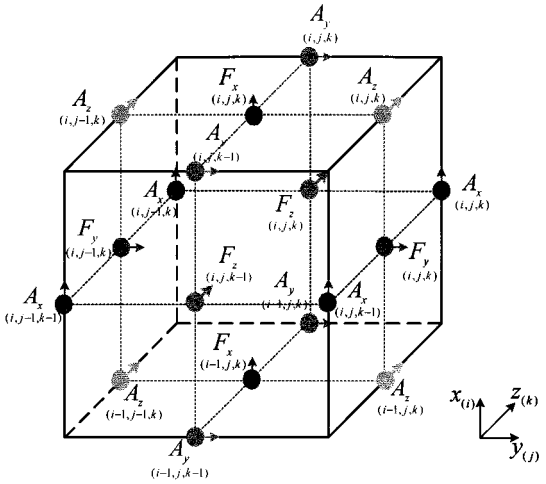

Fig. 2. Discretization cell showing the location in space of the three possible VP pairs in a rectangular coordinate system.

wave equations describing the field propagation inside a domain are complemented by Dirichlet BCs, which are calculated at the domain's boundary via the transition equations discussed in Section III. In practice, a closed-domain surface will never require BCs in terms of normal field components $(D_n,\, B_n)$ only, simply because the domain's VP pair of constant direction can never be normal to the domain boundary S at every point.

The introduction of domains of constant direction of the VP pair in practical algorithms eliminates the complications arising from mode coupling. It makes the proposed theoretical model efficient and applicable to the solution of practical EM problems. It is clearly simpler to implement in cases of predominantly homogeneous regions with large planar interfaces. However, there are no theoretical limits to its implementation to general lossy inhomogeneous problems.

V. Finite-Difference Implementation

The above theory has been implemented in a finite-difference algorithm, in which the domains are either boxes (six-sided rectangular prisms) or planar layers. Their boundaries are always in homogeneous regions. Central differences are used throughout the algorithm, which is based on the finite-difference discretization of the wave equations of the WPs and the transition formulas given in Table I. Every two collinear VPs are displaced by a half-step along all three axes (see Fig. 2). Besides, the magnetic VPs are displaced by a half-step in time with respect to the electric VPs.

The quantities calculated by the algorithm are normalized potential functions such that the finite-difference transition equations, which involve derivatives of both, i.e., the magnetic and electric VPs, manipulate numbers of the same order. The VPs $(A_\xi,\, F_\xi)$ are represented by the quantities

$$\begin{aligned} a_\xi &= \sqrt{Z_0}\,(A_\xi/\mu) \\ A\times\Omega^{1/2} &= W^{1/2} \\ f_\xi &= (F_\xi/\varepsilon)/\sqrt{Z_0} \\ V\times\Omega^{-1/2} &= W^{1/2}. \end{aligned} \tag{28}$$

Here, $Z_0=\sqrt{\mu_0/\varepsilon_0}$ is the intrinsic impedance of vacuum.

In a homogeneous medium, the discretized wave equation, which allows the computation of each WP according to (14), is

$$\begin{aligned} \left(v_x^2\,D_{xx}^2 f + v_y^2\,D_{yy}^2 f + v_z^2\,D_{zz}^2 f\right) \\ -D_{tt}^2 f - \left(s_\varepsilon + s_\mu\right) D_t f - s_\varepsilon s_\mu f = -g. \end{aligned} \tag{29}$$

Here, $D_{\xi\xi}^2$ ($\xi\equiv x$, y, or z) is a second-order finite-difference operator with respect to the variable ξ, D_t is a first-order finite-difference operator with respect to time, f is the respective WP (a_ξ or f_ξ), and g is a normalized source function $g_\xi = J_\xi(v\triangle t)^2\sqrt{Z_0}$ or $g_\xi = J_{m\xi}(v\triangle h)^2/\sqrt{Z_0}$, where $v=c/\sqrt{\varepsilon_r\mu_r}$ is the local speed of light. The rest of the numerical constants are as follows:

$$\begin{aligned} v_\xi &= v\triangle t/\triangle\xi, \qquad \text{where } \xi\equiv x, y, \text{ or } z \\ s_\varepsilon &= \sigma\triangle t/\varepsilon \\ s_\mu &= \sigma_m\triangle t/\mu \end{aligned}$$

There is no need to explicitly calculate the scalar potentials Φ and Ψ, which are related to the VPs via Lorenz gauge (13) unless inhomogeneous lossy problems are solved. In the latter case, the finite-difference implementation requires the explicit computation of the scalar potentials via (13) and their subsequent substitution in (14).

The BCs at dielectric and magnetic interfaces are automatically satisfied if the normal to the interface VP pair is used. The values of the VPs at the interfaces are calculated using the general equations in (14), which take into account the gradients of the material constants. The $F_{\varepsilon n}$ equation at dielectric interfaces and the $A_{\varepsilon n}$ equation at magnetic interfaces do not differ from their respective equations in points of zero gradients $\nabla\varepsilon=0$ and $\nabla\mu=0$. The $A_{\varepsilon n}$ equation at dielectric interfaces differs from the respective zero-gradient equation by its modified ∇^2 operator, as dictated by (14). For example, if $\hat{n}\equiv\hat{x}$, then the Laplacian operator in the $A_{\varepsilon n}$ equation is replaced by

$$\nabla^2 A_{\mu x} + (\nabla\varepsilon)\partial_t\Phi = \nabla_\perp^2 A_{\mu x} + \varepsilon\partial_x\left(\varepsilon^{-1}\partial_x A_{\mu x}\right) \tag{30}$$

where $\nabla_\perp^2=\partial_{yy}^2+\partial_{zz}^2$. The equation of $F_{\varepsilon n}$ at magnetic interfaces is dual to that of $A_{\mu n}$ at dielectric interfaces.

The finite-difference discretization of the three-dimensional wave equation is straightforward. However, the implementation of the transition equations via finite differences at the boundary between two domains deserves more detailed explanation. There are two cases of interest. Case 1 refers to a boundary at which the VP pairs of the two neighboring domains are tangential. Case 2 refers to a boundary at which one of the pairs is normal. Without loss of generality, we will illustrate it with the transition equations at a boundary between two domains: one carrying the $(A_{\mu x},\, F_{\varepsilon x})$ pair and the other one carrying the $(A_{\mu y},\, F_{\varepsilon y})$ pair.

Case 1 will correspond to a boundary at a $z=\text{const.}$ plane. The domains overlap with one cell size. Thus, $(A_{\mu x},\, F_{\varepsilon x})$ are calculated via $(A_{\mu y},\, F_{\varepsilon y})$ one step inside the $(A_{\mu y},\, F_{\varepsilon y})$ domain and vice versa. The normalized WPs are calculated using the following explicit time-stepping discretized equations from

Table I:

$$D_{tt}^2 a_x + (s_\varepsilon + s_\mu) D_t a_x + s_\varepsilon s_\mu a_x = v_x^2 D_{xx}^2 a_x - v_{xy}^2 D_{xy}^2 a_y - v_{z0}(\mu_r \varepsilon_r)^{-1} D_z \cdot \Big\{ \varepsilon_r D_t f_y + s_{\varepsilon 0} f_y \Big\} \quad (31)$$

$$D_{tt}^2 f_x + (s_\varepsilon + s_\mu) D_t f_x + s_\varepsilon s_\mu f_x = v_x^2 D_{xx}^2 f_x - v_{xy}^2 D_{xy}^2 f_y + v_{z0}(\mu_r \varepsilon_r)^{-1} D_z \cdot \Big\{ \mu_r D_t a_y + s_{\mu 0} a_y \Big\} \quad (32)$$

$$D_{tt}^2 a_y + (s_\varepsilon + s_\mu) D_t a_y + s_\varepsilon s_\mu a_y = v_y^2 D_{yy}^2 a_y - v_{yx}^2 D_{yx}^2 a_x + v_{z0}(\mu_r \varepsilon_r)^{-1} D_z \cdot \Big\{ \varepsilon_r D_t f_x + s_{\varepsilon 0} f_x \Big\} \quad (33)$$

$$D_{tt}^2 f_y + (s_\varepsilon + s_\mu) D_t f_y + s_\varepsilon s_\mu f_y = v_y^2 D_{yy}^2 f_y - v_{yx}^2 D_{yx}^2 f_x - v_{z0}(\mu_r \varepsilon_r)^{-1} D_z \cdot \Big\{ \mu_r D_t a_x + s_{\mu 0} a_x \Big\}. \quad (34)$$

Here, in addition to the numerical constants defined in (29), one has to also introduce the following:

$$v_{z0} = c\triangle t/\triangle z$$
$$v_{xy} = v\triangle t/\sqrt{\triangle x \triangle y}$$
$$s_{\varepsilon 0} = \sigma \triangle t/\varepsilon_0, \quad \text{where } \varepsilon_0 \text{ is the permittivity of vacuum}$$
$$s_{\mu 0} = \sigma_m \triangle t/\mu_0, \quad \text{where } \mu_0 \text{ is the permeability of vacuum}$$

Notice that (31) and (32) are the finite-difference representation of the equations in (17), which were used to illustrate the mode equivalence concept in Section III.

In a uniform mesh, the spatial discretization step $\triangle h = \triangle x = \triangle y = \triangle z$ and the time-step $\triangle t$ are related through the constant $q = \triangle h/(c\triangle t)$, where c is the highest velocity of light in the structure. According to Courant's stability condition, $q \geq \sqrt{3}$. In this particular algorithm, q is chosen as $q = 2$, which makes the implementation of Liao's [18] absorbing boundary condition (ABC) very simple.

Consider now Case 2 when the VP pair of one of the domains is normal to the mutual boundary, e.g., a boundary at $x = \text{const}$. While (33) and (34) are still valid, (31) and (32) are not applicable because of the second-order derivatives along the boundary's normal $D_{xx}a_x$ and $D_{xx}f_x$. They are now replaced by the following formulas, which are the finite-difference discretized version of the expressions in (15):

$$v_y^2 D_{yy}^2 a_x + v_z^2 D_{zz}^2 a_x = -v_{xy}^2 D_{xy}^2 a_y - v_{z0}(\mu_r \varepsilon_r)^{-1} D_z \Big\{ \varepsilon_r D_t f_y + s_{\varepsilon 0} f_y \Big\} \quad (35)$$

$$v_y^2 D_{yy}^2 f_x + v_z^2 D_{zz}^2 f_x = -v_{xy}^2 D_{xy}^2 f_y + v_{z0}(\mu_r \varepsilon_r)^{-1} D_z \Big\{ \mu_r D_t a_y + s_{\mu 0} a_y \Big\}. \quad (36)$$

TABLE II
COMPUTATIONAL REQUIREMENTS OF THE FDTD AND THE TDWP ALGORITHMS

	FDTD	TDWP
sum./cell	4×6=24	8×2=16
mult./cell	1×6=6	2×2=4
total/cell	5×6=30	10×2=20
memory/cell	1×6 = 6	2×2 =4

From a computational point-of-view, these equations are quite different from (31) and (32). They require the solution of Poisson's equation at the domain boundary. Finite differences are used again to discretize them. The resultant matrix is inverted offline only once before the time-stepping loop starts.

According to the number of operations per cell, in its finite-difference implementation, the algorithm would require at most two-thirds of the computation time and, at most, two-thirds of the memory requirements of the Yee-cell FDTD algorithm in the general case (see Table II). The savings are very significant for problems, which can be handled by only one of the two WPs in a pair.

Stability criteria, discretization cell size, and excitation waveforms are chosen exactly as in a conventional FDTD algorithm.

VI. NUMERICAL TESTS

There are three important issues that have been tested numerically and will be presented here, i.e., the transition between domains with different direction of the VP pair, the correct field representation at edges and corners, and the VP behavior at material (e.g., dielectric) interfaces.

A. Transitions Between Domains

The transition between VP pairs of different (orthogonal) directions has been tested in homogeneous problems since the domain boundaries in the general algorithm are always at least one cell away from inhomogeneities. One of the test structures is shown in Fig. 3. This is a hollow waveguide of rectangular cross section in the x–y-plane excited with a dominant TE_{z01} distribution of the E_x-component whose waveform is a sine wave modulated by a Blackman–Harris window [19]. The input and output sections are the domains of the (A_z, F_z) pair. The middle section supports: 1) the (A_z, F_z) pair in the first experiment; 2) the (A_y, F_y) pair in the second experiment; and 3) the (A_x, F_x) pair in the third experiment. The waveguide ports are terminated with Liao's fourth-order ABC [18]. The higher order Liao's ABC causes instabilities. In all three experiments, the wave impedance and wavelength were calculated to compare with the analytical formulas. The results of all three experiments are given for the frequency band between the cutoff frequency of the dominant TE_{01} mode and the cutoff of the TE_{02} mode. They are practically indistinguishable from each other, and they only slightly deviate from the analytical calculations at low frequencies close to cutoff (see Fig. 3). Notice that the dominant TE_{01} mode is fully described by only one WP: either F_z or F_y or A_x due to its independence from the x-coordinate.

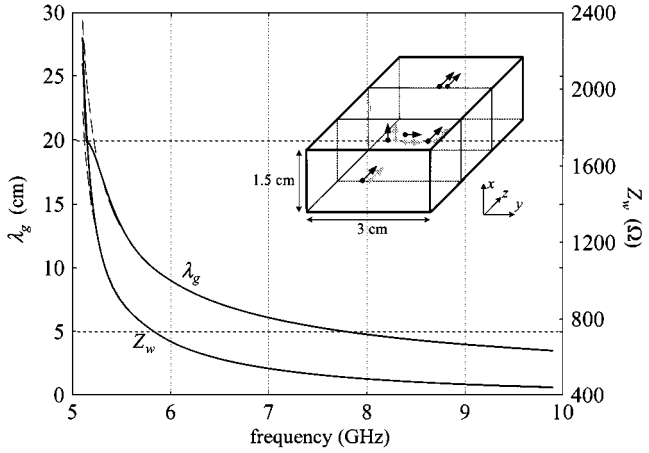

Fig. 3. Impedance and wavelength computations for a waveguide using a middle domain with three different VP pairs. With lines: TDWP. With dashed-line: analytical calculations.

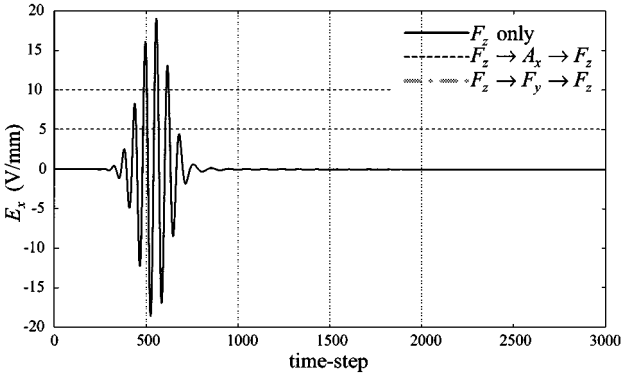

Fig. 4. Time sample of the incident pulse (sine wave modulated by Blackman–Harris window) in the hollow waveguide exciting the structure in the frequency band from 5 to 10 GHz.

The incident pulse (reflections are below 0.25%) is shown in Fig. 4 for the three cases of domain segmentation. These three transient responses are also indistinguishable from each other.

A second test was performed on an open problem: an infinitesimally thin dipole antenna, where the middle domain centered onto the antenna has all of its six walls bordering domains whose VPs are orthogonal to those in the middle domain. The current distribution (at three different wavelengths) is compared with the current distribution obtained when the problem is solved using only one potential, i.e., the magnetic VP component $A_{\mu z}$ tangential to the dipole (see Fig. 5).

B. Dielectric Interfaces and Conducting Edges

The performance of the algorithm in structures with conducting wedges has been tested with an H-plane rectangular bend and E-plane rectangular bend of the waveguide considered before (see Fig. 3).

The structure of the H-plane waveguide bend was divided into three domains, i.e., the input waveguide section with the (A_z, F_z) pair, the bend section with the (A_x, F_x) pair, and the output waveguide section with the (A_y, F_y) pair. The edge of the bend is along the x-axis (see Fig. 6). The S-parameters were

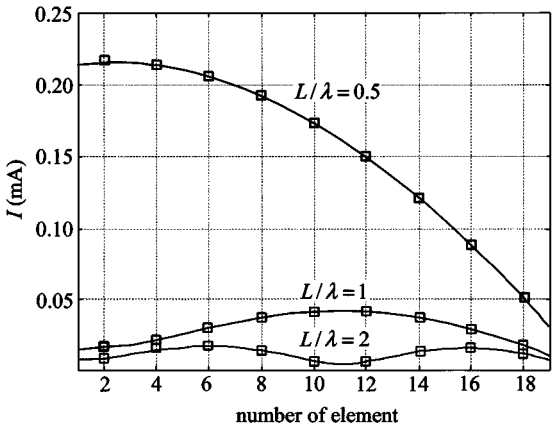

Fig. 5. Current distribution along half the length of a wire dipole. With lines: single potential. With points: computational region divided into seven domains.

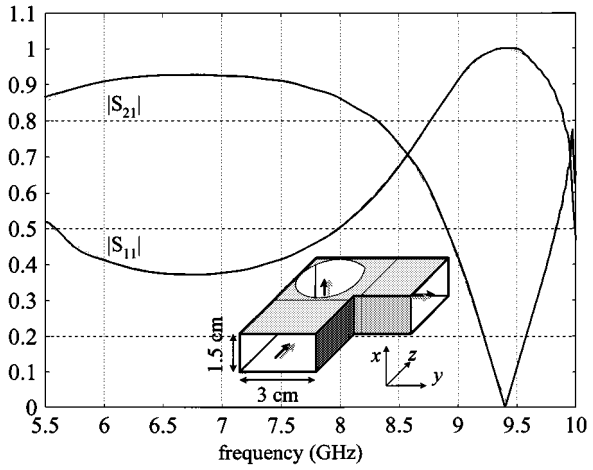

Fig. 6. Magnitudes of the S-parameters of the H-plane right-angle waveguide bend. With lines: TDWP. With dashed lines: Agilent HFSS simulation.

calculated and compared with those produced by Agilent HFSS[1] (a finite-element method (FEM)-based simulator). The results are given in Fig. 6.

Similarly, the E-plane waveguide bend was divided into three domains, i.e., the input waveguide section with the (A_z, F_z) pair, the bend section with the (A_y, F_y) pair, and the output waveguide section with the (A_x, F_x) pair. The edge of the bend is along the y-axis (see Fig. 7). A comparison with results generated by Agilent HFSS is given in Fig. 7.

A relevant comparison should be made here between the behavior of the field and the behavior of the potentials at perfectly conducting edges. The potential pair does not have any singularity unlike the field components orthogonal to the edge. The magnetic potential decreases smoothly to zero as it approaches the edge, while the electric potential rises gradually in amplitude to produce a zero normal derivative.

The correct representation of the field propagation at a dielectric interface by the normal to the interface VP pair was tested on an example, which has analytical solution, i.e., the partially filled waveguide of rectangular cross section. The structure's dimensions are shown in Fig. 8. In this example, the solution

[1]HP HFSS, ver. 5.2, HP EEsof, Santa Rosa, CA, 1998.

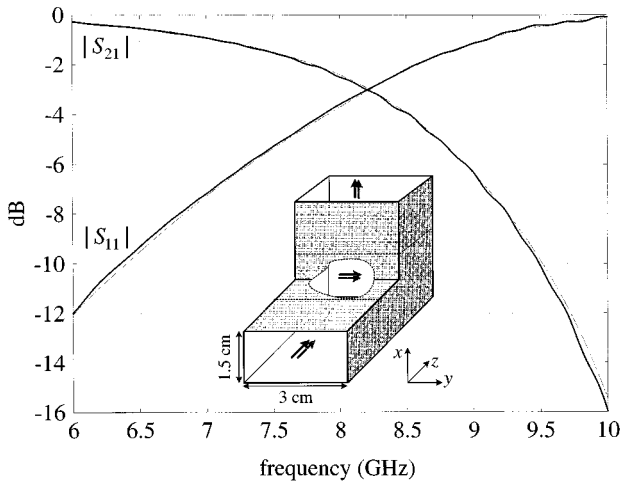

Fig. 7. Magnitudes of the S-parameters of the E-plane right-angle waveguide bend. With lines: TDWP. With dashed lines: Agilent HFSS simulation.

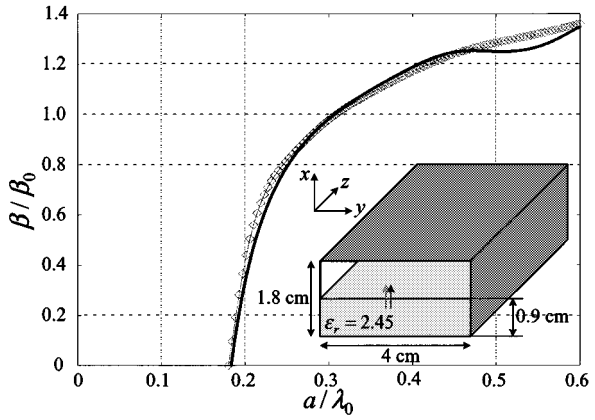

Fig. 8. Normalized phase constant of the partially filled waveguide. With lines: TDWP. With lines–points: analytical solution.

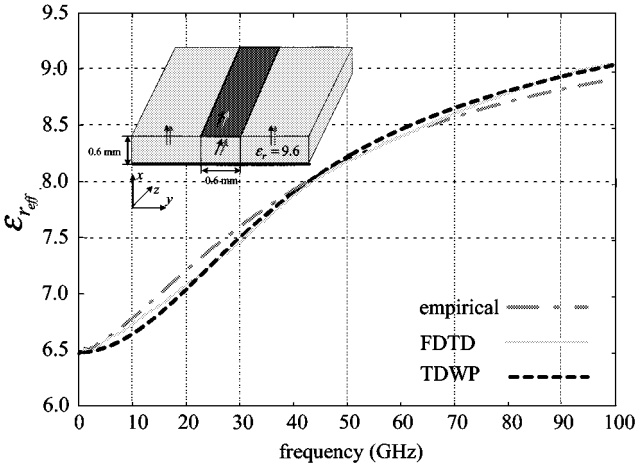

Fig. 9. Effective dielectric constant of the microstrip line. Comparison between the empirical formula of Hammerstad and Jensen (dashed–dotted line), FDTD algorithm [20] (line), and the TDWP algorithm (dashed line).

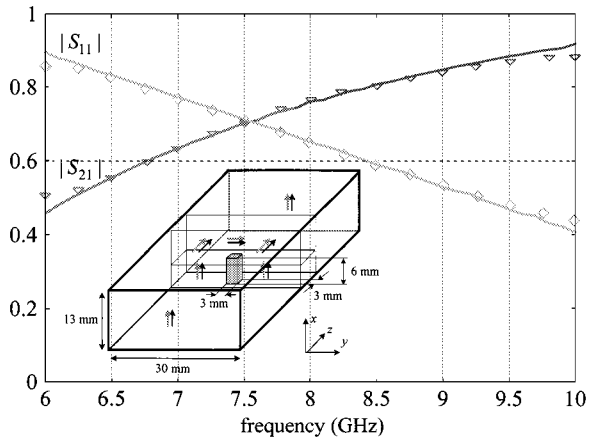

Fig. 10. S-parameters for the dominant TE_{01} mode of the rectangular waveguide post. With points: Agilent HFSS. With lines: TDWP.

for the TM_x modes only will be shown, which requires a single WP, i.e., A_x. No segmentation into domains is necessary. The analytical solution, which produces the guide phase constant β_g, is explained in detail in [1]. Fig. 8 shows the dispersion of the guide phase constant β_g for the dominant TM_{x01} mode whose cutoff frequency is approximately $f_c^{\mathrm{TM}_{x01}} \simeq 3.15$ GHz. Both analytical and computed values are plotted together for comparison. At the higher end of the frequency band, certain deviation is observed from the expected values of the dominant-mode phase constant β_g, which is attributed to the existence of the higher-order TM_{x02} mode whose cutoff frequency is approximately $f_c^{\mathrm{TM}_{x02}} \simeq 6.3$ GHz, which corresponds to $a/\lambda_c^{\mathrm{TM}_{x02}} \simeq 0.38$. In order to accurately represent all mode-dependent dispersion parameters of a high-frequency structure, two-dimensional Fourier transform with respect to the two spatial coordinates in the reference plane/port has to be applied to the field distribution. However, this feature has not yet been developed.

The microstrip line example tested the algorithm not only for the correct representation of the field propagation at dielectric interfaces, but also at conducting edges (the microstrip line is of infinitesimal thickness). The propagation characteristics of the line were calculated for the structure shown in Fig. 9. Fig. 9 also shows the calculated effective dielectric constant as a function of frequency. Comparison is made with empirical results obtained by the formulas reported in [20], and with the results generated by the FDTD algorithm [21]. A sheet of x-directed currents right beneath the strip excites the structure. The excitation function in time is a Gaussian pulse.

The performance of the algorithm was also tested on a structure involving conducting corners, i.e., waveguide post in a hollow waveguide (see Fig. 10). Here, all three pairs have to be used in order to avoid ill-posed BCs at the edges of the waveguide post, which has a rectangular cross section. Careful choice of the excitation function was made in order to excite the dominant TE_{01} mode only. The excitation pulse had a band-limited spectrum whose spectral components were above 10% of the maximum between 6–10 GHz. The computed magnitudes of the S-parameters are plotted together with the results obtained by Agilent HFSS in Fig. 10.

VII. Conclusion

In this paper, the construction of solutions to general transient EM problems in terms of two collinear VPs has been considered. It has been shown that as long as the gradient of the EM

properties of the analyzed region coincides with the direction of the VPs, the solution can be built in terms of only two scalar quantities, i.e., the magnitudes of the VPs. Such a restriction on the gradient of the constitutive parameters would severely limit the applicability of the method if VPs of fixed direction were used throughout the volume. However, it has been shown that there are no theoretical obstacles for the utilization of VPs of different directions in different subregions of the analyzed volume. The method has been implemented in a finite-difference algorithm, which has better computational efficiency than the conventional FDTD technique. Current research efforts are directed toward further generalization of the method to include the theory of equivalent EM sources. Successful implementation of this theory would lead to enhanced versatility of the TDWP algorithm with respect to inhomogeneities and boundary shapes.

ACKNOWLEDGMENT

The author wishes to thank and acknowledge Prof. W. S. Weiglhofer, Department of Mathematics, University of Glasgow, Glasgow, U.K., for his valuable advice and comments.

REFERENCES

[1] R. F. Harrington, *Time–Harmonic Electromagnetic Fields*. New York: McGraw-Hill, 1961, p. 131.
[2] D. S. Jones, *Acoustic and Electromagnetic Waves*. New York: Oxford Univ. Press, 1986, pp. 27–29.
[3] E. Whittaker, *A History of the Theories of Aether & Electricity*. New York: Harper Bros., 1960, vol. 1, pp. 409–410.
[4] S. Przeździecki and W. Laprus, "On the representation of electromagnetic fields in gyrotropic media in terms of scalar Hertz potentials," *J. Math. Phys.*, vol. 23, pp. 1708–1712, Sept. 1982.
[5] J. J. Sein, "Solutions to time–harmonic Maxwell equations with a Hertz vector," *Amer. J. Phys.*, vol. 57, pp. 834–839, Sept. 1989.
[6] W. S. Weiglhofer, "Scalar Hertz potentials for linear bianisotropic mediums," in *Electromagnetic Fields in Unconventional Materials and Structures*, O. N. Singh and A. Lakhtakia, Eds. New York: Wiley, 2000, pp. 1–37.
[7] I. V. Lindell and F. Olyslager, "Potentials in bi-anisotropic media," *J. Electromagn. Waves Applicat.*, vol. 15, pp. 3–18, 2001.
[8] W. S. Weiglhofer, "Scalar Hertz potentials for nonhomogeneous uniaxial dielectric–magnetic mediums," *Int. J. Appl. Electromagn. Mechan.*, vol. 11, pp. 131–140, 2000.
[9] N. Georgieva and E. Yamashita, "Time-domain vector-potential analysis of transmission-line problems," *IEEE Trans. Microwave Theory Tech.*, vol. 46, pp. 404–410, Apr. 1998.
[10] F. De Flaviis, M. G. Noro, R. E. Diaz, G. Franceschetti, and N. G. Alexopoulos, "A time-domain vector potential formulation for the solution of electromagnetic problems," *IEEE Microwave Guided Wave Lett.*, vol. 8, pp. 310–312, Sept. 1998.
[11] R. E. Diaz, F. DeFlaviis, M. Noro, and N. G. Alexopoulos, "A new computational electromagnetics method based on discrete mathematics," in *Frontiers in Electromagnetics*, D. H. Werner and R. Mittra, Eds. Piscataway, NJ: IEEE Press, 2000, ch. 17.
[12] D. Krupežević, V. Branković, and F. Arndt, "The wave-equation FD–TD method for the efficient eigenvalue analysis and S-matrix computation of waveguide structures," *IEEE Trans. Microwave Theory Tech.*, vol. 41, pp. 2109–2115, Dec. 1993.
[13] P. H. Aoyagi, J. F. Lee, and R. Mittra, "A hybrid Yee algorithm/scalar-wave equation approach," *IEEE Trans. Microwave Theory Tech.*, vol. 41, pp. 1593–1600, Sept. 1993.
[14] N. Georgieva and Y. Rickard, "The application of the wave potential functions to the analysis of transient electromagnetic fields," in *IEEE MTT-S Int. Microwave Symp. Dig.*, vol. 2, 2000, pp. 1129–1132.
[15] K. S. Yee, "Numerical solution of initial boundary value problems involving Maxwell's equations in isotropic media," *IEEE Trans. Antennas Propagat.*, vol. 14, pp. 302–307, May 1966.
[16] J. C. Strikwerda, *Finite Difference Schemes and Partial Differential Equations*. Belmont, CA: Wadsworth , 1989, pp. 158–163.
[17] C. A. Balanis, *Advanced Engineering Electromagnetics*. New York: Wiley, 1989.
[18] Z. P. Liao, H. L. Wong, Y. Baipo, and Y. Yifan, "A transmitting boundary for transient wave analyzes," *Scientia*, vol. XXVII, no. 10, pp. 1063–1076, Oct. 1984.
[19] F. J. Harris, "On the use of windows for harmonic analysis with the discrete Fourier transform," *Proc. IEEE*, vol. 66, pp. 51–83, Jan. 1978.
[20] E. Hammerstad and O. Jensen, "Accurate models for microstrip computer-aided design," in *IEEE MTT-S Int. Microwave Symp. Dig.*, 1980, pp. 407–409.
[21] Y. Qian and T. Itoh, *FDTD Analysis and Design of Microwave Circuits and Antennas (Software and Applications)*. Tokyo, Japan: Realize, 1999.

Natalia K. Georgieva (S'93–M'97) received the Dipl. Eng. degree from the Technical University of Varna, Varna, Bulgaria, in 1989, and the Ph.D. degree from the University of Electro-Communications, Tokyo, Japan, in 1997.

In July 1999, she joined the Department of Electrical and Computer Engineering, McMaster University, Hamilton, ON, Canada, where she is currently an Assistant Professor. Her research interests include computational electromagnetics, analysis and modeling of high-frequency structures, as well as CAD approaches to microwave/millimeter-wave devices and antennas.

Dr. Georgieva was the recipient of the 1998–1999 Natural Sciences and Engineering Research Council of Canada (NSERC) post-doctoral fellowship and the 2000 NSERC University Faculty Award.